Improved long-range reactive bond-order potential for carbon. II. Molecular simulation of liquid carbon

Luca M. Ghiringhelli,[1] Jan H. Los,[2] A. Fasolino,[1,2] and Evert Jan Meijer[1]
[1]*van't Hoff Institute for Molecular Sciences, Universiteit van Amsterdam, Nieuwe Achtergracht 166, 1018 WV Amsterdam, The Netherlands*
[2]*Institute for Molecules and Materials, Radboud University Nijmegen, Toernooiveld 1, 6525 ED Nijmegen, The Netherlands*
(Received 15 July 2005; published 2 December 2005)

Using the recently developed state-of-the-art empirical bond-order potential (LCBOPII), presented in the companion paper [Los *et al.*, Phys. Rev. B **72**, 214102 (2005)], we study liquid carbon by Monte Carlo simulation. We determined the equation-of-state and local structure over a wide range of temperatures (4000–15 000 K) and pressures (up to 300 GPa). Comparison of the equation-of-state and local structure along the 6000 K isotherm with benchmark *ab initio* molecular dynamics data shows that LCBOPII provides accurate predictions. The local coordination varies gradually from mixed two- and three-fold, via dominantly threefold, to mainly fourfold with increasing temperature and pressure. This provides evidence that there is no liquid-liquid phase separation as confirmed by the regular behavior of the pressure-density relations along the isotherms in the range of 5000–15 000 K. We provide an accurate fit of the pressure-temperature-density equation-of-state that may serve as a reference for future studies of liquid carbon.

DOI: 10.1103/PhysRevB.72.214103 PACS number(s): 81.05.Uw, 61.20.Ja, 34.20.Cf, 71.15.Pd

I. INTRODUCTION

The liquid phase of carbon provides one of the most severe benchmarks for accuracy and transferability of the long-range carbon bond-order potential (LCBOPII) introduced in the companion paper.[1] The ability of carbon of having twofold (sp), threefold (sp^2), and fourfold (sp^3) coordinated atoms makes this element relevant in different fields of fundamental science and technology. This is also the most challenging property of this element, in the perspective of the design of transferable and accurate potentials. The bond-order potentials (BOPs) introduced in the past[2–5] proved to be not sufficiently transferable to describe the liquid phase over a wide range in temperature (T) and pressure (P). Some of those potentials showed spurious first order liquid-liquid phase transitions (LLPT) associated with a change of dominant coordination. It has long been suspected that elemental carbon might exhibit a LLPT.[6,7] Classical simulations[8] based on the Brenner bond-order potential with torsional terms[2,3] predicted a LLPT from a twofold to a denser, fourfold coordinated liquid upon compression, with the liquid-liquid coexistence line starting at a maximum in the graphite melting line and ending in a critical point. The short-range potential of Ref. 4 (REBO) and the short-range potential (CBOP) presented in Ref. 5 show[9] a transition to a graphitelike liquid along the 6000 K isotherm. Subsequent more accurate density functional theory based molecular dynamics (DFMD) simulations[10,11] did not show a LLPT, indicating that the predicted LLPT is spurious and should be attributed to shortcomings of the employed BOPs.

Recently improved BOPs have been introduced. AIREBO and AIREBOII of Refs. 12 and 13, and the potential introduced by us[11] (LCBOPI$^+$) do not yield a LLPT. The design of LCBOPI$^+$, an extension of an earlier potential introduced by some of us,[5] is extensively discussed in the companion paper.[1] The LCBOPI$^+$ was used in previous studies of the carbon phase diagram[14] and the structural properties of the liquid.[11] Still, the liquid structure of the LCBOPI$^+$ was not completely satisfactory and further improvements were introduced as described in the companion paper,[1] yielding the LCBOPII. LCBOPII has been validated to some experimental data, albeit at less extreme conditions than those of the liquid state. For example, in the companion paper[1] we have shown that LCBOPII reproduces accurately experimental data for the reconstructed 111 diamond surface. Note also that LCBOPI$^+$, which is related to LCBOPII, reproduces the experimental graphite-diamond melting accurately.[14]

The purpose of the present paper is twofold. First, we will compare the LCBOPII liquid with density functional theory based molecular dynamics (DFMD) simulations and simulation data from the literature. Note that no reliable experimental data are available at these extreme conditions, i.e., a temperature of 6000 K and pressures from ~1 to ~150 GPa. Second, we extend the DFMD data for the liquid to a wider range of the phase diagram employing LCBOPII, exploiting the fact that LCBOPII simulations are orders of magnitude faster than DFMD simulations.

The present paper is organized as follows. In Sec. II we describe the simulation methods employed, both for the classical potentials (i.e., the LCBOPII and the LCBOPI$^+$) and for DFMD. In Sec. III we describe the equation of state [EOS, $P=P(\rho,T)$] of liquid carbon, and propose a polynomial fit for the EOS. In Sec. IV we present the distribution of sp-, sp_2-, and sp_3-coordinated sites over a wide range of densities and temperatures. Our analysis shows an impressive agreement with the reference data. Subsequently, in Sec. V we present the radial distribution functions (rdfs) at several densities and temperatures. We discuss both total rdfs and partial rdfs for atoms with specific coordinations. In Sec. VI we briefly report the behavior of the angular distribution functions at different state points. Sections III–VI are naturally split into two parts, the first comparing LCBOPII with refer-

 ©2005 The American Physical Society

ence data, and the second with properties for state points not extensively covered in literature. We conclude in Sec. VII with a brief summary, conclusions, and an outlook.

II. METHODS

All the simulations with the LCBOPII are performed using the Metropolis Monte Carlo (MC) algorithm, in the constant volume, number of particles, and temperature (NVT) ensemble. Systems consisted of 128 and 1000 atoms in a periodically replicated cubic box. The initial configurations were generated starting from a cubic arrangement that was melted at the highest probed temperature (15 000 K). Subsequently, the temperature for the systems was fixed at seven values (15 000, 10 000, 8000, 7000, 6000, 5000, and 4500 K), and the systems were equilibrated for 5×10^5 MC moves per particle, followed by a production run of 10^6 MC moves per particle. The 128 particles samples were used to compare the results of the LCBOPII with calculated DFMD data or with data taken from literature. The 1000-particle MC simulations with LCBOPII were used to generate the bulk of the data presented in this paper. The local structure of the liquid, i.e., the coordination fractions, and the radial and angular distribution functions show a negligible dependence on the system size. However, some collective properties, such as pressure and internal energy, show a small but non-negligible system size dependence. Typically, the 128- and 1000-particle systems show a pressure difference of 3% and an internal energy difference of 0.3%. We selected 15 densities[34] ranging from 3.99×10^3 to 1.73×10^3 kg/m^3. The lowest density was chosen to be near the graphite melting line.[14] The pressure was calculated via virtual volume displacements. If V is the volume of the sample, its potential energy is U_V at a given configuration. The energy of the sample rescaled to a volume V' is then $U_{V'}$. In the limit of $V'/V\rightarrow1$, and with V' fixed as well as V, it holds:

$$P=\rho k_B T-\frac{\langle U_{V'}-U_V\rangle}{V'-V} \tag{1}$$

where $\langle\cdots\rangle$ denotes the average in the NVT ensemble. This method avoids the measurement of forces, not needed in MC simulations.

A small part of the simulated state points is in the region of the phase diagram where the liquid is metastable with respect to diamond. We have used direct free-energy difference calculations to estimate the liquid freezing line for LCBOPII from the freezing line of LCBOPI$^+$ of Ref. 14, without repeating the full, laborious, calculation. The following relation yields the difference in chemical potential for the two potentials at a given (P,T) state point:

$$\beta\mu_{II}=-\frac{1}{N}\ln\langle\exp(-\beta(U_{\mathrm{LCBOPII}}-U_{\mathrm{LCBOPI^+}}))\rangle_{I^+}, \tag{2}$$

where $\langle\cdots\rangle_{I^+}$ denotes the NPT ensemble average with the LCBOPI$^+$, and $\beta=1/k_BT$. If we apply this to a state point on the LCBOPI$^+$ freezing line where both coexisting phases have equal chemical potential ($\Delta\mu^{I+}=0$), we obtain the chemical potential difference $\Delta\mu^{II}$ between the two phases for the LCBOPII. Subsequently, keeping the pressure fixed, the coexistence temperature for the LCBOPII can be determined using

$$\left.\frac{\partial\beta\Delta\mu^{II}}{\partial\beta}\right|_P=h_1^{II}-h_2^{II}, \tag{3}$$

where h_1^{II} and h_2^{II} are the specific enthalpies $[h=(U+PV)/N]$ of the two coexisting phases that are evaluated in two additional simulations with the LCBOPII.

Using this procedure we determined the liquid-diamond freezing temperature for the LCBOPII, starting from the LCBOPI$^+$ liquid-diamond coexistence point at $T=6000$ K and $P=59.44$ GPa. Employing Eq. (2) we obtained $\beta\Delta\mu_{II}=0.205$ at this state point. It is important to note that the distributions of both the internal energy and the volume for LCBOPI$^+$ and LCBOPII show significant overlap, and that the difference $(U_{\mathrm{LCBOPII}}-U_{\mathrm{LCBOPI^+}})$ is bound within reasonable values: so the LCBOPI$^+$ and LCBOPII showed to be rather similar in this respect. Both features are required for an accurate estimate of the chemical potential difference using Eq. (2). Subsequently, the coexistence temperature for LCBOPII was determined ($T=5505$ K) employing a predictor-corrector algorithm to solve $\Delta\mu_{II}(P,T)=0$ using Eq. (3). The slope of the diamond-liquid melting line for the LCBOPII was determined by performing simulations of the liquid and diamond at the LCBOPII coexistence point and applying the Clausius-Clapeyron equation $dT/dP=T\Delta v/\Delta h$. Here Δv indicates the volume difference per particle. The slope was evaluated as 28.04 K/GPa and appears to be near the value of 28.97 K/GPa for LCBOPI$^+$ at the same pressure.

The DFMD simulations were performed in the NVT ensemble using the Car-Parrinello[15] method as implemented in the CPMD package.[16] The electronic structure was calculated using the Kohn-Sham formulation of density functional theory employing the gradient-corrected density functional in its BP[17,18] parametrization. The system consisted of 128 atoms in a periodically replicated cubic cell. The Kohn-Sham states were expanded in a plane-wave basis set sampled at the Γ point in the Brillouin zone, and truncated at a kinetic energy (E_{cut}) of 35 Ry. This cutoff ensured the convergence of the binding energy for small clusters within 5 kJ/mol per bond. We restricted the number of electronic states to those of the valence electrons by means of semilocal norm-conserving Martins-Troullier pseudopotentials.[19] We constructed the pseudopotential with a valence-electron configuration s^2p^2, using core-radii of 1.23 a.u. for both the $l=s$ and $l=p$ terms. The pseudopotential was transformed into the Kleinman-Bylander form[20] with $l=p$ as the local term. The ionic temperature was controlled via a Nosé-Hoover thermostat.[21] As in our DFMD simulations liquid carbon is metallic, a proper implementation of the Car-Parrinello method requires the electronic degrees of freedom to be coupled to a thermostat. Here we coupled a Nosé-Hoover chain thermostat to the electronic degrees of freedom with a target energy of 0.25 eV and a coupling frequency of 15 000 cm^{-1}. The target energy was estimated using the procedure proposed by Blöchl and Parrinello.[22] The coupling

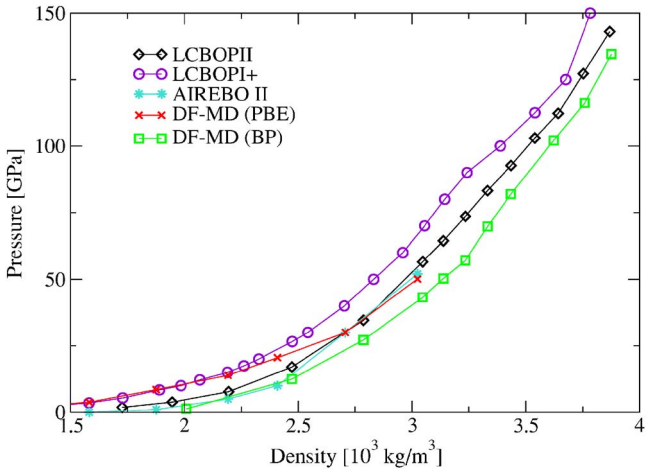

FIG. 1. (Color online) Calculated equations of state at 6000 K for LCBOPII and DFMD employing the BP functional. The statistical error for the pressure is smaller than the symbol size. Note that the DFMD results for the nine highest densities are also reported in Ref. 11. For comparison, results obtained with the LCBOPI$^+$ (Ref. 11), the AIREBOII potential (Ref. 13), and DFMD employing the BPE functional (Ref. 10) are shown. From these last two series, a point at 1.28×10^3 kg/m^3 is not shown.

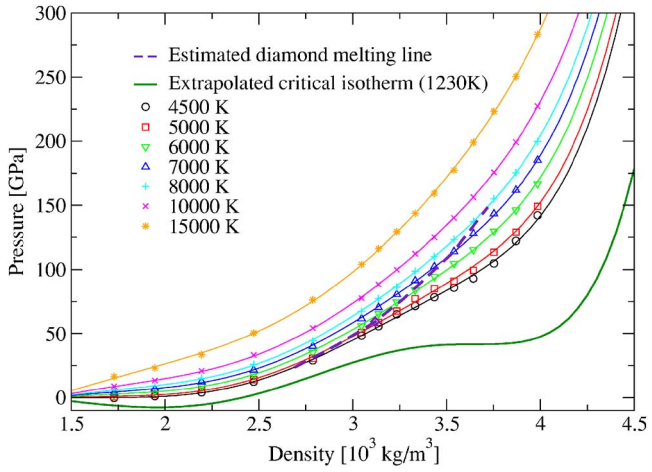

FIG. 2. (Color online) Equations of state for the LCBOPII at seven different temperatures: 4500 K (circles), 5000 K (squares), 6000 K (diamonds), 7000 K (triangles), 8000 K (plus), 10 000 K (crosses), and 15 000 K (stars). Each temperature is sampled at 15 different densities. Error bars, not shown, are within the symbol size. The relative error is around 1% at the highest pressure and increases up to 10% at the lowest (i.e., smaller than 5 GPa). The thick line at the bottom is the extrapolated critical isotherm, at 1230 K. It has a horizontal inflection point at density 3.66×10^3 kg/m^3 and pressure 41.74 GPa. The dashed line is the estimated diamond melting line, starting from the calculated point shown as a diamond (at 5505 K, 59.4 GPa, and 3.12×10^3 kg/m^3, see Sec. II), and prolonged assuming constant dT/dP.

frequency of 15 000 cm^{-1} was chosen to be within the dominant frequencies of the wave functions, determined from a DFMD simulation with fixed ion positions. The initial points were taken from equilibrated LCBOPII configurations at the same density and temperature. These were equilibrated for about 0.5 ps, followed by a production run of 5 ps. For the DFMD simulations, the pressure is evaluated as

$$P = \rho k_B T + \frac{1}{3}\langle \mathrm{Tr}\,\mathbf{\Pi}\rangle + P_{corr} \tag{4}$$

where $\langle \mathrm{Tr}\,\mathbf{\Pi}\rangle$ is the ensemble average of the sum of the diagonal elements of the stress tensor $\mathbf{\Pi}$.[23] P_{corr} is a correction term accounting for the fact that only the bonding energy and not the (total) Kohn-Sham energy is converged for a plane-wave basis set usually employed in DFMD simulation: this gives rise to a spurious contribution to the virial, known as the Pulay stress.[24] This contribution acts as a downward shift. To correct for the Pulay stress, we performed short simulations at each density, at $E_{\mathrm{cut}}=120$ Ry, for which the total energy is almost converged and $P_{\mathrm{corr}}\sim 0$. P_{corr} at $E_{\mathrm{cut}}=35$ Ry is then the difference in $\langle 1/3\ \mathrm{Tr}\,\mathbf{\Pi}\rangle$ between the simulations at 35 and 120 Ry plane-wave cutoff energy.

III. EQUATION OF STATE

A. Comparison

Figure 1 shows $\rho-P$ state points along the 6000 K isotherm obtained with DFMD and the LCBOPII. For comparison we have also plotted results from literature: data obtained with DFMD employing the BPE functional,[10] and data obtained with LCBOPI$^+$ (Ref. 11) and AIREBOII.[13] The difference in calculated pressures between the two DFMD simulations should be attributed to the use of a different functional. Differences in E_{cut} and pseudopotential should not contribute significantly to this discrepancy, as both setups yielded good bonding energies. Compared to the DFMD results, LCBOPII improves the performance of the LCBOPI$^+$ by lowering the pressure towards the DFMD result and by suppressing the decrease of the slope of the density-pressure curve around 3.3×10^3 kg/m^3. The results for the AIREBOII potential[13] are similar to that of LCBOPII. The early short-range potentials CBOP and REBO do reproduce the DFMD data for the EOS reasonably well for low densities, but fail at higher densities beyond the spurious LLPT. For REBO this is shown in Ref. 11.

B. Predictions

In Fig. 2 we have plotted the pressure-density curves of the LCBOPII for seven isotherms from 4500 to 15 000 K. Also the estimated coexistence line is plotted. In the stable region all curves show a regular monotonic increase of the slope of the curve. In the undercooled region we observe for the 4500 and 5000 K isotherms, in a small density region around 3.3×10^3 kg/m^3, a decrease of the slope. For LCBOPI$^+$ this wiggling of the pressure-density curve was a pronounced feature at 6000 K and associated with a rapid switching of the dominant coordination from three- to fourfold. For LCBOPII the same coordination change occurs in the wiggling region, around 3.3×10^3 kg/m^3, of the 4500 and 5000 K isotherms (see below).

TABLE I. Parameters of Eq. (5).

c_1:	$-3.22435447999\times10^{7}$	J
c_2:	$9.88711221869\times10^{3}$	J K^{-1}
c_3:	$-6.05245942342\times10^{1}$	J K^{-2}
c_4:	$1.63510457127\times10^{5}$	J K^{-3}
c_5:	$2.53078007240\times10^{4}$	J m^3 kg^{-1}
c_6:	$-9.47985686674\times10^{1}$	J m^3 kg^{-1} K^{-1}
c_7:	$1.20616311340\times10^{-3}$	J m^3 kg^{-1} K^{-2}
c_8:	$-3.42300962915\times10^{-8}$	J m^3 kg^{-1} K^{-3}
c_9:	$-2.49596407210\times10^{1}$	J m^6 kg^{-2}
c_{10}:	$-2.04475278536\times10^{-4}$	J m^6 kg^{-2} K^{-1}
c_{11}:	$-5.00834553350\times10^{-7}$	J m^6 kg^{-2} K^{-2}
c_{12}:	$1.41814229613\times10^{-11}$	J m^6 kg^{-2} K^{-3}
c_{13}:	$5.24835967149\times10^{-2}$	J m^9 kg^{-3}
c_{14}:	$2.60371540562\times10^{-6}$	J m^9 kg^{-3} K^{-1}
c_{15}:	$-3.08370110012\times10^{-6}$	J m^{12} kg^{-4}
c_{16}:	$-2.44955788712\times10^{-10}$	J m^{12} kg^{-4} K^{-1}
c_{17}:	$5.24072792404\times10^{-9}$	J m^{15} kg^{-5}
c_{18}:	$-3.22777913222\times10^{-14}$	J m^{15} kg^{-5} K^{-1}
ρ_0:	1.35694366721 kg m^{-3}	

We employed a polynomial function to fit the calculated LCBOPII equation of state:

$$P(\rho,T) = (\rho-\rho_0)(c_1 + c_2T + c_3T^2 + c_4T^3) + (\rho-\rho_0)^2(c_5 + c_6T + c_7T^2 + c_8T^3) + (\rho-\rho_0)^3(c_9 + c_{10}T + c_{11}T^2 + c_{12}T^3) + (\rho-\rho_0)^4(c_{13} + c_{14}T) + (\rho-\rho_0)^5(c_{15} + c_{16}T) + (\rho-\rho_0)^6(c_{17} + c_{18}T). \quad (5)$$

The parameters of the fit function are given in Table I and are obtained by minimizing the square of the difference between the calculated and fitted pressures. The functional form is fully empirical and designed to have a minimum number of parameters needed to describe all the features of the data points. The fit could possibly be employed outside the region of calculated state points. A reasonable extension for the density would be a range between $\sim1.5\times10^3$ and $\sim4.5\times10^3$ kg/m^3.

The polynomial fit reproduces the wiggling of the 4500 and 5000 K isotherms for the undercooled liquid. It is tempting to explore the behavior of the fit at lower temperatures, beyond the region of calculated state points. At these temperatures the liquid is even more undercooled. With decreasing temperatures the wiggles become more pronounced, yielding an inflection point with zero slope in the $P-\rho$ plane for the 1230 K isotherm at 3.66×10^3 kg/m^3, and 41.74 GPa. This behavior is typical for the critical isotherm. At lower temperatures, the isotherms of the fit function show a van der Waals loop, indicating a first-order phase transition associated with a density change. However, in our simulations the system freezes below 4000 K, especially at densities higher than 3×10^3 kg/m^3. Hence it would be rather speculative to propose the presence of a liquid-liquid phase transition. Still it might be interesting to explore the undercooled liquid by considering a (much) larger system size and performing careful annealing to see if a scenario similar to that of liquid water, with its speculated liquid-liquid phase transition hidden in the glass region,[25–27] would appear.

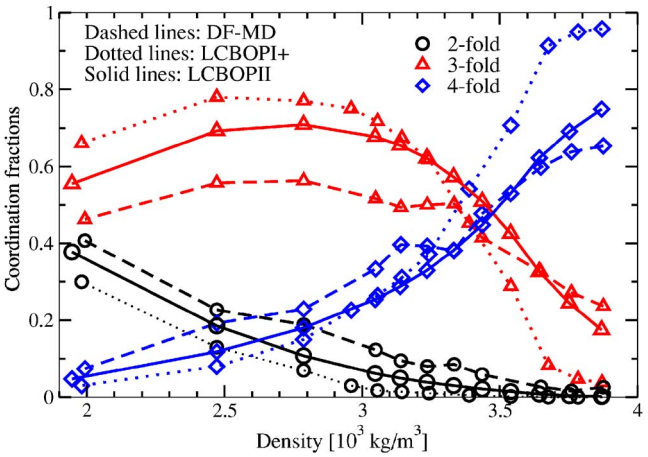

FIG. 3. (Color online) Comparison of coordination fractions at 6000 K between the LCBOPII (solid lines), the LCBOPI$^+$ (dotted lines), and reference data coming from our own DFMD (dashed lines). Data at density 2.79×10^3 kg/m^3 and higher are the same as shown in Ref. 11. Data at the two lowest densities were calculated for this publication for both DFMD and the LCBOPI$^+$. Circles always represents twofold sites, triangles threefold, and diamonds fourfold. Fivefold sites are not shown but can be deduced by subtraction, since no atoms with a single bond (onefold) or sixfold sites were observed at these densities. The error bars, not shown, are within the symbol size, $\sim$0.01 for the semiempirical potentials and $\sim$0.02 for the DFMD points.

IV. COORDINATION

A. Comparison

The local coordination of atoms is determined by counting neighbors using the smoothed cutoff functions defined for the LCBOPII. Specifically, we employed the following cutoff radii: atoms closer than 0.17 nm to a given atom are counted as its integer neighbors, atoms further than 0.22 nm are not counted, and atoms in between are partially counted, by means of the cutoff function S_N^{down} defined in the companion paper.[1] This implies that a coordination fraction equal to, e.g., three can be given also by two integer and two partial neighbors. Here we should note that in literature various alternative definitions of the coordination fractions are employed. These may yield different values for a similar atomic configuration. Hence a direct comparison of coordination fractions with literature data should be done with some care, a point also noted by Marks.[28] Figure 3 shows the coordination fractions calculated with LCBOPII and DFMD along the 6000 K isotherm. For comparison also the results for LCBOPI$^+$ from Ref. 11 are shown. We see that, except for a slight overestimation of the threefold fractions in the low-density regime, the LCBOPII results reproduce the DFMD data very well, both for the density dependence as for the absolute values. The LCBOPII improves the predictions of

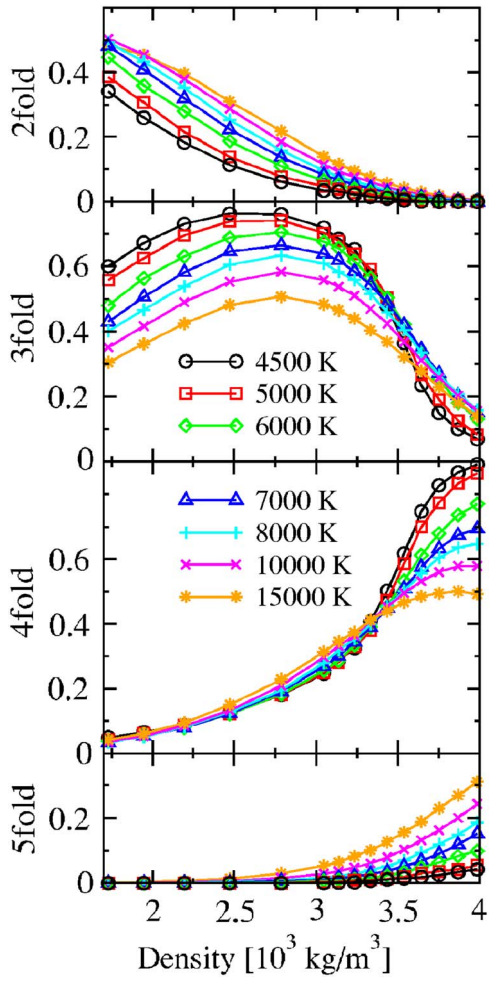

FIG. 4. (Color online) Coordination fractions at seven temperatures according to the LCBOPII. The symbol code is the same as for Fig. 2. Each panel shows a different coordination fraction interval, but vertical axes share the same unit, so that they can be directly compared. The error bars, not shown, would be smaller than the symbol size, typically around 0.01.

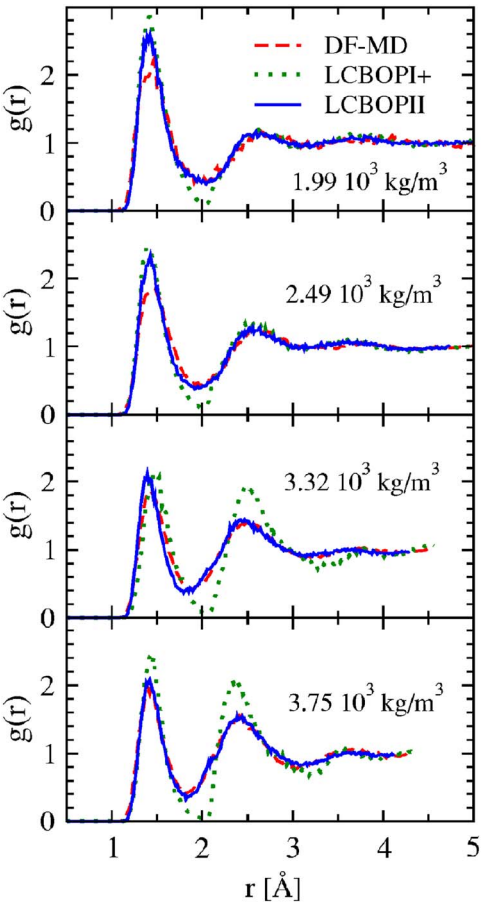

FIG. 5. (Color online) Comparison of the radial distribution functions at 6000 K and four selected densities between the LCBOPII (solid lines), the LCBOPI+ (dotted lines), and the reference data taken from our own DFMD simulations (dashed lines).

the LCBOPI+: at densities up to $\sim 3.4\times10^3$ kg/m^3 the LCBOPII predicts less threefold and more two- and four-fold sites, thus getting closer to the DFMD data. At higher densities, where the LCBOPI+ overestimated the fourfold fraction, the coordination fractions predicted by LCBOPII almost perfectly recover the DFMD data. Fivefold coordinated atoms (not shown in Fig. 3) only appear in the high-density region. At 3.75×10^3 kg/m^3 the fraction for LCBOPII is 0.1, slightly larger than the DFMD value of 0.07. Note that this is a remarkable achievement of the potential, as the structures used to develop LCBOPII did not have fivefold coordination. We also note that in the high density range, short-range BOPs hardly show coordination beyond three. For the LCBOPI+ the fivefold fraction remained negligible. The appearance of fivefold coordinated structures in LCBOPII calculations is due to the presence of the middle range part (V_{ij}^{mr}: see Sec. II D of the companion paper) in the potential and to the softening of angular correlations. In fact, in older BOPs as well as in the LCBOPI, a small angle such as 60° had a significant energetic penalty, fitted to a 12-fold structure (i.e., an fcc lattice) that applied also for fivefold sites. With the LCBOPII the penalty at small angle for this lower coordination has been reduced [see Eq. (12) in the companion paper]. As already shown in Ref. 11 the REBO potential yields a negligible fourfold fraction at all the densities: the threefold atoms replace the twofold upon increasing density, until the spurious LLPT at which all the atoms become threefold. The LLPT appears also for CBOP, but the fraction of fourfold atoms raises to ~10% before the transition. No data regarding coordinations in the liquid are available for AIREBOII, while the environment dependent potential (EDIP) introduced by Marks[29] is similar to LCBOPII in reproducing the DFMD coordination fractions at 5000 K.[28]

B. Predictions

In Fig. 4 we show the average coordination fractions at several temperatures. For clarity two-, three-, four-, and fivefold coordination fractions are shown in different panels, respectively, from top to bottom. The fraction of sixfold coordinated atoms was negligible at all simulated state points. Onefold coordinated atoms appear only in a small amount (a few percent) at the lowest densities, and are not shown. Considering the density dependence, we observe, for all tempera-

tures, that the atoms are mainly two- and three-fold coordinated in the low density region, with the twofold sites gradually replaced by three- and four-fold sites upon increasing density. At 6000 K the two- and three-fold fractions match around $\rho=1.73\times10^3$ kg/m^3. Note that the maximum of the threefold fraction is at $\rho\sim2.75\times10^3$ kg/m^3 for all temperatures. The threefold sites are replaced by fourfold sites over a relatively short density range around $\rho=3.4\times10^3$ kg/m^3. The fivefold fraction only appears with a significant fraction in the high-density region and shows a marked temperature dependence. This is related to the stronger temperature dependence of the fourfold fraction in the high-density region.

V. RADIAL DISTRIBUTION FUNCTION

A. Comparison

In Fig. 5 we present the radial distribution functions (rdfs) $g(r)$ obtained for the LCBOPII, LCBOPI$^+$, and DFMD at four selected densities along the 6000 K isotherm. Taking DFMD as a reference, we see that LCBOPII is a major improvement with respect to the LCBOPI$^+$. In particular the minimum between the first and second shell is now properly described. Here we should note that the rdf and the coordination fractions at $\rho=3.75\times10^3$ kg/m^3 were used as a test system in the development of the potential. The figures also show that LCBOPII reproduces the DFMD values for the peak positions, and the height of the second and third peak. Only the first-peak height is slighly overestimated by LCBOPII, consistent with the fact that LCBOPII showed larger values for the higher coordination numbers (Fig. 3).

Figure 6 compares the LCBOPII rdfs for a liquid at 2.9×10^3 kg/m^3 at four different temperatures with 64-atom DFMD data from Ref. 30, calculated using the local density approximation (LDA) functional. This figure makes clear that, up to 12 000 K, also the temperature dependence is well reproduced by LCBOPII. The temperature dependence is typical for a liquid: the peak heights decrease with increasing temperature, while minima increase, indicating a gradual loss of structure. It is striking that all the curves cross at the same points where the rdf equals 1. In fact, at ~0.165, ~0.230, and ~0.285 nm, the value of the rdf is 1, regardless of the temperature.

B. Predictions

Figure 7 shows radial distribution functions for a wide range of densities at 6000 K. We see that the position of the first peak is rather constant, whereas the position of the second peak moves markedly inwards with increasing density. This is consistent with the findings of other DFMD[30] and tight binding[31] calculations of liquid carbon, and is also seen in simulations of other covalently bonded liquids.[32] The height of the first peak decreases significantly when the density goes from 1.73×10^3 to 2.79×10^3 kg/m^3. This should be attributed to the change in the coordination pattern, going from mixed two- and three-fold to mainly threefold. Upon further increase of the density it keeps the same height. In contrast, the second peak height increases gradually upon increasing density, while the dip between these two peaks smoothly decreases.

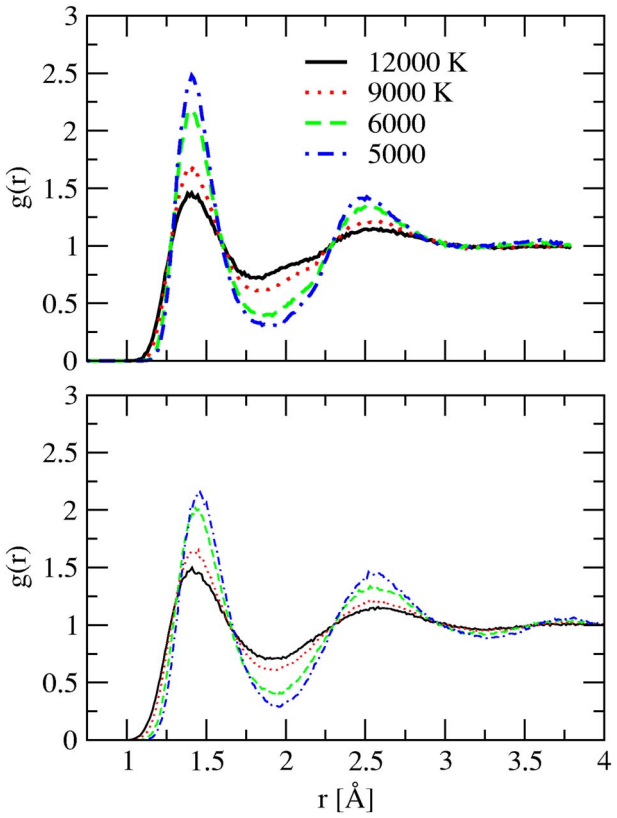

FIG. 6. (Color online) Comparison of the radial distribution functions at 2.9×10^3 kg/m^3 and four temperatures between the LCBOPII (top panel) and reference data taken from Ref. 30 (bottom panel). Solid lines are at 12 000 K, dotted lines at 9000 K, dashed lines at 6000 K, and dotted-dashed lines are at 5000 K.

C. Partial radial distribution functions

We performed a further analysis of the liquid structure by examining the spatial correlation between the positions of carbon atoms with a specific coordination. We determined partial radial distribution functions (prdfs) $g_{ij}(r)$, defined as the probability of finding a j-fold site at a distance r from an i-fold site. We have found some dependence of the prdfs on the value of the cutoff radii used in the definition of neighbors. However, important features such as the positions of peaks and minima, and the relative height of the peaks inside the same g_{ij}, appear to be rather independent of the cutoff radii. The results we present are obtained using the same definition of cutoff radius given in Sec. IV.

In Figs. 8 and 9 we show the partial radial distribution functions at 6000 K at two selected densities. At a density of 1.73×10^3 kg/m^3 the dominant coordinations are two- and three-fold both appearing with an equal fraction. Figure 8 shows that the positions of the first peaks of g_{22} and g_{33} are at 0.133 and 0.142 nm, typical for a sp and sp^2 type of bonding, respectively.

This agrees with the DFMD results of Ref. 33 yielding an average bond length from g_{22} of 0.135 nm at

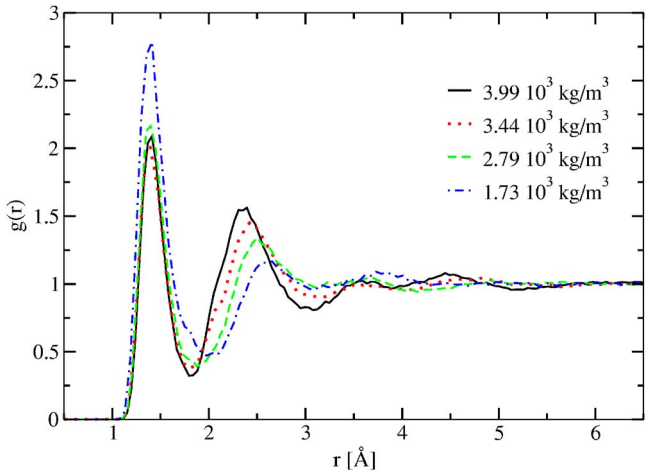

FIG. 7. (Color online) Radial distribution functions at 6000 K and four selected densities for the LCBOPII. Density 1.73 and 3.99×10^3 kg/m^3 are, respectively, the lowest and the highest sampled. At the lowest density twofold and threefold are present with the same fraction. Density 2.79×10^3 kg/m^3 shows the maximum in the fraction of threefold coordinated atoms. Density 3.44×10^3 kg/m^3 has almost the same amount of three- and four-fold sites. These same densities are analyzed in their angular distribution functions (Fig. 10), two of them in their partial distribution functions (Figs. 8 and 9).

2.00×10^3 kg/m^3 and 5000 K. The prdf among twofold coordinated atoms (g_{22}), apart from the first peak arising from nearest neighbors, is rather structureless. This suggests that there are hardly any straight chains of three or more subsequent twofold coordinated carbons. Conversely, a second and a third peak in the radial distribution appear among the threefold coordinated atoms (g_{33}). The prdfs of Fig. 8 suggest the liquid structure to be a mixture of short bent chains and rings that are often mutually connected: this picture is supported

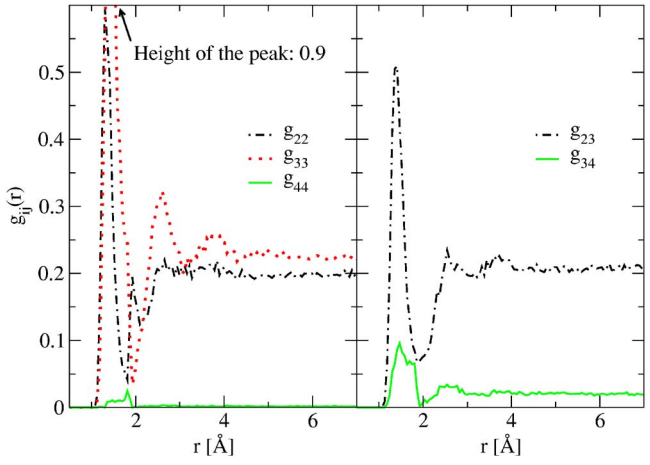

FIG. 8. (Color online) Partial radial distribution functions (g_{ij}) at 1.73×10^3 kg/m^3 and 6000 K for the LCBOPII. The left panel is for the diagonal terms (i.e., $i=j$): the dashed-dotted line is for the g_{22}, the dotted line for the g_{33}, the solid line for the g_{44}. The right panel is for the cross terms (i.e., $i\neq j$): the dashed-dotted line is for the g_{23}, the solid line is for the g_{34}. All the g_{ij} that are not shown are negligible. The total rdf is given by $g=\Sigma_i g_{ii}+2\Sigma_i\Sigma_{j\neq i}g_{ij}$.

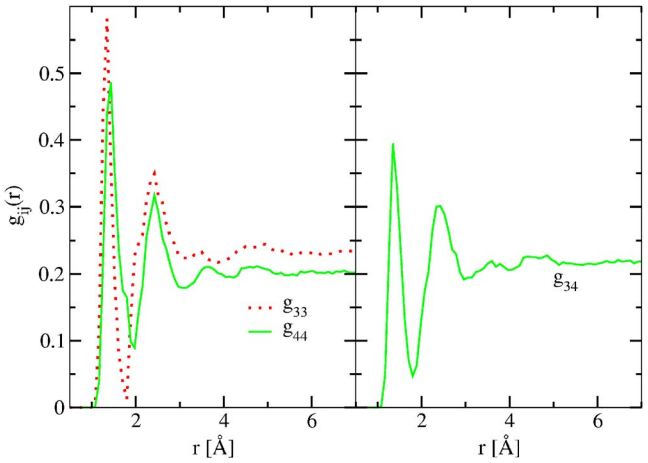

FIG. 9. (Color online) Partial radial distribution functions (g_{ij}) for LCBOPII at 3.44×10^3 kg/m^3 and 6000 K, with almost equal fraction of three- and four-fold coordinated atoms. The left panel is for the diagonal terms (i.e., $i=j$): the dotted line for the g_{33}, the solid line for the g_{44}. The right panel is for the (cross) term g_{23} (i.e., $i\neq j$): All the g_{ij} that are not shown are negligible. The total rdf is given by $g=\Sigma_i g_{ii}+2\Sigma_i\Sigma_{j\neq i}g_{ij}$.

by a visual inspection of liquid configurations. Some of the chains end at a onefold site. The relatively large first peak of g_{34} shows that the small fraction of fourfold coordinated atoms is mainly bonded to threefold coordinated atoms. Occasionally there appear isolated dimers and bent trimers, as can be inferred from g_{11} (not shown) and visual inspection.

At the higher density of 3.44×10^3 kg/m^3 the dominant coordinations are three- and four-fold, both almost equally represented. Figure 9 shows substantial structure for all prdfs with almost equal peak heights, indicating good mixing among three- and four-fold coordinated atoms. For g_{44} the position of the first two peaks and minima coincide with those of diamond. Also the ratio of the heights of the first two peaks, ~1.6, is similar to that of diamond. These observations are consistent with the observation of Ref. 11 that a mainly fourfold coordinated liquid has a diamondlike structure up to the second shell of neighbors. The positions of the first peak and minimum of g_{33} are slightly but noticeably smaller than those of g_{44}. The small differences among the prdfs in the positions of peaks and minima should be attributed to differences in bond length for sp_2 and sp_3 type of bonding.

At the highest density considered (3.99×10^3 kg/m^3) the liquid is mainly fourfold coordinated with a small fraction of three- and five-fold coordinated atoms. The prdfs at this density (not shown) reveal a local diamondlike structure for the fourfold coordinated atoms, and show that the three- and five-fold coordinated atoms are mainly connected to fourfold coordinated atoms.

The partial distribution functions at temperatures above and below 6000 K (not shown here) have a temperature dependence similar to that of the total rdfs (Fig. 6), with increasing temperature, peaks tend to flatten and broaden, but in such a way that the radial positions of the extrema are preserved.

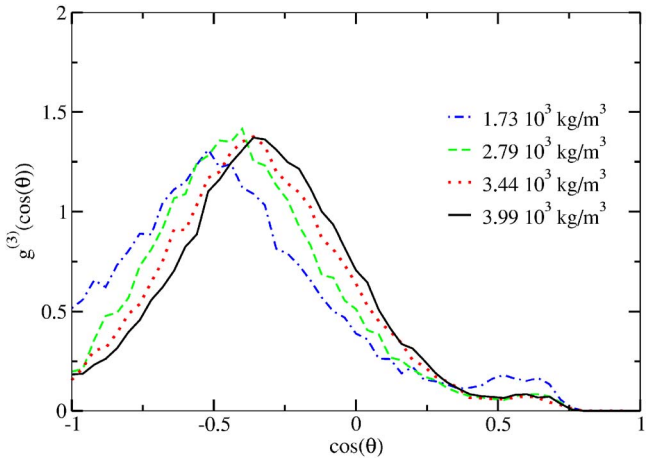

FIG. 10. (Color online) Angular distribution functions at 6000 K and four different densities for the LCBOPII. The line code is the same as in Fig. 7.

VI. ANGULAR DISTRIBUTION FUNCTION

The angular distribution function $g^{(3)}(\cos(\theta))$ is determined as the distribution of the cosine of angles between bonds to neighboring atoms. Again, we should keep in mind that there is some arbitrariness in the definition of neighboring atoms: we used the same definition specified in Sec. IV. The angular distributions for LCBOPII agree very well with our DFMD[9,11] results, for which we could use the same definition of cutoff radius as for the LCBOPII. Compared to LCBOPI$^+$, this is a significant improvement as the results of Ref. 11 showed that there was only a qualitative agreement between LCBOPI$^+$ and DFMD, with LCBOPI$^+$ underestimating the presence of sub 90° structures. The improvement of LCBOPII over LCBOPI$^+$ should be attributed to the softening of the angular part in the potential giving a lower energy for fourfold coordinated structures at small angles. Figure 10 shows the angular distributions at 6000 K at the same four densities of Fig. 7. At highest density (3.99×10^3 kg/m^3) the angular distribution is peaked near the tetrahedral angle $[\cos(\theta)=-0.3]$, typical for diamond. Decreasing the density to 1.73×10^3 kg/m^3 the peak position moves towards a value $\cos(\theta) \simeq -0.5$, i.e., the angle typical for graphite. For all densities the distribution near the peak is rather symmetric with a Gaussian-like shape. Note also that the distributions are broad, and cover angles from 50° to 180°. At 1.73×10^3 kg/m^3 the tail at small angles features a local maximum around 50°. We relate this peak, that has also been observed in our[9,11] as well as in earlier DFMD simulations,[28,30] to nearly equilateral triangular structures. These peculiar triangular structures, that are present at all densities, occasionally merge in pairs in a rhomboidal structure. It is remarkable that LCBOPII is also able to recover this feature.

We also determined the angular distribution of bonds to the second neighbors. At 6000 K, the most prominent feature is a peak at 60° which appears also prominently in the angular distribution of graphite and diamond. Together with an average coordination of 12 s neighbors for the highest density considered this suggests, as earlier noticed by us,[11] that metastable liquid carbon has a diamondlike structure.

VII. CONCLUSIONS

In summary, in this paper we showed the performance for liquid carbon of the recently introduced LCBOPII.[1] We explicitly compared the equation of state, the coordination fraction, and the radial distribution function of the LCBOPII with reference data from density functional based simulations. We extended the analysis of the liquid in regions of pressure and temperature not covered from other reference data. On the basis of the equation of state, the coordination fractions, the radial distributions function, and the angular distribution functions, we show the extreme accuracy and transferability of the LCBOPII. Looking at the calculated equation of state, we argue that a (first order) liquid-liquid phase transition could only be found in a deeply undercooled liquid. It is not clear if these conditions can ever be reached. In simulations, this would at least require a very large system size and a careful cooling from a stable liquid. On the basis of the partial radial distribution function at a density where three- and four-fold sites are equally present, we provide a further argument against a phase separation: the alikeness of the partial radial distribution functions suggest, at 6000 K, a negligible strain energy amongst atoms of three- and four-fold coordination.

The present results are a first application of LCBOPII in studies of condensed phase carbonic materials under extreme conditions. It is well suited for the study of various other types of carbonic materials. Future extensions of LCBOPII could involve the incorporation of other elements such as hydrogen, oxygen, nitrogen, and various metals. This would open the way to the study of advanced nanosized materials.

ACKNOWLEDGMENTS

This work is part of the research program of the "Stichting voor Fundamenteel Onderzoek der Materie (FOM)," which is financially supported by the "Nederlandse Organisatie voor Wetenschappelijk Onderzoek (NWO)." J.H.L and A.F. acknowledge NWO Project No. 015.000.031 for financial support. E.J.M. acknowledges the Royal Netherlands Academy of Art and Sciences for financial support. We acknowledge support from the Stichting Nationale Computerfaciliteiten (NCF) and the Nederlandse Organisatie voor Wetenschappelijk Onderzoek (NWO) for the use of supercomputer facilities. We acknowledge Bastiaan Huisman and Sara Iacopini for useful discussions.

[1] J. H. Los, L. M. Ghiringhelli, E. J. Meijer, and A. Fasolino, preceding paper, Phys. Rev. B **72**, 214102 (2005).
[2] D. W. Brenner, Phys. Rev. B **42**, 9458(E) (1990); D. W. Brenner, Phys. Rev. B **46**, 1948 (1992).
[3] D. W. Brenner, J. H. Harrison, C. T. White, and R. J. Colton, Thin Solid Films **206**, 220 (1991).
[4] D. W. Brenner, O. A. Shenderova, J. A. Harrison, S. J. Stuart, B. Ni, and S. B. Sinnott, J. Phys.: Condens. Matter **14**, 783 (2002).
[5] J. H. Los and A. Fasolino, Phys. Rev. B **68**, 024107 (2003).
[6] A. Ferraz and N. H. March, Phys. Chem. Liq. **8**, 289 (1979).
[7] M. van Thiel and F. H. Ree, Phys. Rev. B **48**, 3591 (1993).
[8] J. N. Glosli and F. H. Ree, Phys. Rev. Lett. **82**, 4659 (1999).
[9] L. M. Ghiringhelli, Ph.D. thesis, On the nature of phase transition in covalent liquids, University of Amsterdam, The Netherlands, 2005.
[10] C. J. Wu, J. N. Glosli, G. Galli, and F. H. Ree, Phys. Rev. Lett. **89**, 135701 (2002).
[11] L. M. Ghiringhelli, J. H. Los, E. J. Meijer, A. Fasolino, and D. Frenkel, Phys. Rev. B **69**, 100101(R) (2004).
[12] S. J. Stuart, A. B. Tutein, and J. A. Harrison, J. Phys. Chem. **14**, 6472 (2000).
[13] O. Kum, F. H. Ree, S. J. Stuart, and C. J. Wu, J. Chem. Phys. **119**, 6053 (2003).
[14] L. M. Ghiringhelli, J. H. Los, E. J. Meijer, A. Fasolino, and D. Frenkel, Phys. Rev. Lett. **94**, 145701 (2005).
[15] R. Car and M. Parrinello, Phys. Rev. Lett. **55**, 2471 (1985).
[16] CPMD, version 3.3, developed by J. Hutter, A. Alavi, T. Deutsch, M. Bernasconi, S. Goedecker, D. Marx, M. Tuckerman, and M. Parrinello, MPI für Festkörperforschung and IBM Zurich Research Laboratory, 1995–1999.
[17] A. D. Becke, Phys. Rev. A **38**, 3098 (1988).
[18] J. P. Perdew, Phys. Rev. B **33**, 8822 (1986); J. P. Perdew, Phys. Rev. B **34**, 7406(E) (1986).
[19] N. Troullier and J. L. Martins, Phys. Rev. B **43**, 1993 (1991).
[20] L. Kleinman and D. M. Bylander, Phys. Rev. Lett. **48**, 1425 (1982).
[21] W. G. Hoover, Phys. Rev. A **31**, 1695 (1985).
[22] P. E. Blöchl and M. Parrinello, Phys. Rev. B **45**, 9413 (1992).
[23] D. Marx and J. Hutter, in *Modern Methods and Algorithms of Quantum Chemistry Proceedings*, Second Edition, edited by J. Grotendorst (Forschungszentrum Jülich, Jülich, Germany 2000), it can be found at http://www.fz-juelich.de/nic-series/.
[24] P. Dacosta, O. H. Nielsen, and K. Kunc, J. Phys. C **19**, 3163 (1986).
[25] O. Mishima and H. E. Stanley, Nature (London) **396**, 329 (1998).
[26] H. E. Stanley, S. V. Buldyrev, M. Canpolat, O. Mishima, M. R. Sadr-Lahijany, A. Scala, and F. W. Starr, Phys. Chem. Chem. Phys. **2**, 1551 (2000).
[27] G. Franzese, G. Malescio, A. Skibinsky, S. Buldyrev, and H. Stanley, Nature (London) **409**, 692 (2001).
[28] N. A. Marks, J. Phys.: Condens. Matter **14**, 2901 (2002).
[29] N. A. Marks, Phys. Rev. B **63**, 035401 (2001).
[30] A. Harada, F. Shimojo, and K. Hoshino, J. Non-Cryst. Solids **74**, 2017 (2005) and private communication.
[31] J. R. Morris, C. Z. Wang, and K. M. Ho, Phys. Rev. B **52**, 4138 (1995).
[32] J. Kōga, H. Okumura, K. Nishio, T. Yamaguchi, and F. Yonezawa, Phys. Rev. B **66**, 064211 (2002).
[33] G. Galli, R. M. Martin, R. Car, and M. Parrinello, Phys. Rev. B **42**, 7470 (1990).
[34] The complete list of densities, in units of 10^3 kg/m^3, is 3.99, 3.87, 3.75, 3.64, 3.54, 3.44, 3.33, 3.24, 3.14, 3.05, 2.79, 2.47, 2.19, 1.95, and 1.73. Points are naturally thicker where the $|dT/dP|$ is higher, see Sec. III.